Angewandte Chemie
Eine Zeitschrift der Gesellschaft Deutscher Chemiker

Supporting Information

Combining Metabolic Engineering and Electrocatalysis: Application to the Production of Polyamides from Sugar

Miguel Suastegui[+], *John E. Matthiesen*[+], *Jack M. Carraher, Nacu Hernandez, Natalia Rodriguez Quiroz, Adam Okerlund, Eric W. Cochran, Zengyi Shao,* and Jean-Philippe Tessonnier**

anie_201509653_sm_miscellaneous_information.pdf

Supporting Information

This PDF file includes:

Materials and Methods

1. Metabolic Engineering and Fermentation
2. Electrocatalytic Hydrogenation
3. Separations
4. Polymer Synthesis

Tables S1 to S5

Figs. S1 to S12

References

Materials and Methods

1. Metabolic Engineering and Fermentation

1.1 Flux balance analysis

Flux balance analysis calculations were performed using MATLAB (Mathworks, Natick, MA) and the COBRA toolbox add-in [1]. The yeast genome-scale model iMM904 was utilized for the analysis [2]. The heterologous pathway to produce MA was added to the iMM904 model as described by Curran *et al.* [3]. The glucose and oxygen uptake rates were set to 20 and 2 mmol gDW^{-1} h^{-1}, respectively [2]. The solution to the linear problem was calculated with the gurobi linear solver.

Initially, the linear system was optimized to maximize the production of biomass. This theoretical value was then set as constraint and flux variability analysis (FVA) was carried out (yielding WT scenario). To simulate the production of muconic acid (MA), the flux to biomass was constrained to 20% of the theoretical maximum, and MA was set as the target reaction. FVA was performed with the new constraints (yielding MA scenario) and the flux through each reaction was compared to the WT scenario. The results of this analysis are displayed in Fig. S1.

1.2 Strains and media

S. cerevisiae strain InvSc1 (*MATa his3D1 leu2 trp1-289 ura3-52 MA*T *his3D1 leu2 trp1-289 ura3-52*) was used as the host for MA production. *S. cerevisiae* YSG50 (*MATα, ade2-1, ade3Δ22, ura3-1, his3-11, 15, trp1-1, leu2-3,112 and can1-100*) was used as the DNA assembly host. YPAD was composed of 1% yeast extract, 2% peptone, 0.01% adenine, and 2% dextrose. Synthetic complete dropout media were composed of 0.5% ammonium sulfate, 0.16% yeast nitrogen without amino acid and ammonium sulfate, 2% or 4% dextrose, and Complete Supplement Mixture lacking the corresponding auxotrophic nutrient (uracil, tryptophan, leucine, histidine, or in combination). *Escherichia coli* BW25141 was cultured in Luria Bertani (LB) media supplemented with 100 μg ml^{-1} ampicillin. Bacteria and yeast were cultured in an orbital shaker incubator at 250 rpm, 37 °C and 30 °C, respectively.

1.3 Plasmid construction

All the strains constructed in this work derive from *S. cerevisiae* InvSc1 (Table S1). Gene knockouts were performed by homologous recombination of a functional *ura3* cassette flanked with 500 bp of the upstream and downstream regions of the target gene. To remove the *ura3* cassette from the *pdc1* loci, a 1000 bp DNA fragment composed of contiguous upstream and downstream *pdc1* regions (500 bp each) was transformed. To remove *ura3* from the *aro1* locus, an *aroY* cassette flanked with upstream and downstream regions of *aro1* was transformed. Selection in SC+Ura+FOA media resulted in colonies with the desired knockout. Confirmation of the knockouts was done by diagnostic PCR. These yielded strain InvSc1 Δ*pdc1* and InvSc1 *aro1::aroY*. The primers were synthesized by IDT Technologies (Coralville, IA); a list of primers for the knockout experiments is shown in Table S2.

All the plasmids in this work were constructed following the DNA Assembler technique [4] in the strain *S. cerevisiae* YSG50. *E. coli* BW25141 was used for plasmid enrichment. The list of plasmids constructed in this work is listed in Table S3. The sequence of the genes that conformed the MA pathway were obtained from the previous work in *S. cerevisiae* [3] and synthesized by GenScript (Piscataway, NJ), including *Podospora anserina* Pa_5_5120 (*AROZ*), encoding 3-dehydroshikimate dehydratase; *Klebsiella pneumoniae AROY*, encoding protocatechuic acid decarboxylase, and *Candida albicans* (*HQD2)*, encoding 1,2-catechol dioxygenase. Endogenous genes were amplified from *S. cerevisiae* YSG50 genomic DNA.

A series of helper plasmids containing constitutive promoters and terminators were used to assemble the expression cassettes (Table S3). PCR was performed with Q5 High-Fidelity DNA polymerase from New England Biolabs (Ipswich, MA) following the user's manual. Fermentas FastDigest enzymes from LifeTechnologies (Grand Island, NY) were used for restriction digestion of DNA. DNA recovery from agarose gels was performed with QIAGEN Gel Extraction Kit (Valencia, CA).

1.4 Construction of a panel of plasmids for overexpressing *ARO1* variants

A panel of plasmids was constructed to force the entrance of carbon towards 3-dehydroshikimic acid (DHS). All plasmids had the multiple-copy plasmid pRS426 GPDp-*Xho*I-PYKt as backbone. Initially the wild type *aro1* gene was amplified from *S. cerevisiae* YSG50 and cloned into pRS426 GPDp-*Xho*I-PYKt, yielding pRS426 GPDp-*aro1*-PYKt.

To halt the conversion of DHS into shikimate, it is necessary to engineer the pentafunctional enzyme ARO1. To determine the substrate binding and catalytic site of ARO1, the sequence was aligned with the dehydroquinate dehydratase genes sourced from bacteria and plant. The alignment showed 100% homology in the catalytic regions and it was determined that the residues K1370 and D1409 in the *S. cerevisiae* ARO1 are the substrate binding and catalytic site, respectively (Fig. S3). Both residues were substituted to alanine by PCR. Two different plasmids were assembled, each containing a different *aro1* mutant, namely, pRS426 $aro1_{K1370A}$ and pRS426 $aro1_{D1409A}$. In parallel, an alternative strategy consisted in overexpressing the *E. coli* genes *aroB* and *aroD,* encoding the enzymes dehydroquinate synthase and dehydroquinate dehydratase. These genes were codon optimized for expression in *S. cerevisiae* and synthesized as gBlocks by IDTDNA, and cloned downstream of the constitutive promoters TEF1p and PYK1p, respectively. The expression cassettes were assembled in pRS246 vector after digestion with *BamH*I, yielding pRS426 *hdqs-hdqd*. To construct the plasmids pRS426 $Aro1_{K1370A}$-*hdqs-hdqd* and pRS426 $Aro1_{D1409A}$-*hdqs-hdqd*, the *aro1* mutant plasmids were cleaved with *BamH*I, and assembled with the gene cassettes obtained from pRS426 *hdqs-hdqd* digested with *Afl*II in yeast.

1.5 Physiological characterization of strains

The specific growth rates of the wildtype InvSc1 and the knockout strains were studied by culturing the strains in YPAD media. The starting OD_{600} was set to 0.2 and samples were taken every 2 hours during the first 12 hours of growth. The absorbance values were measured by Cary 50-Bio UV/Vis spectrophotometer from Agilent Technologies (Santa Clara, CA). Semi logarithmic plots (log OD_{600} vs time) were constructed and the values of the slope were used to determine the specific growth rates. To calculate the biomass yield ($Y_{x/s}$), a conversion value of 0.4 g biomass L^{-1} OD_{600}^{-1} was used. Table S4 shows the growth values for the aforementioned strains.

1.6 Small-scale fermentation

To test the production of MA, seed cultures of the engineered strains were inoculated from frozen stocks into 3 mL of the corresponding drop out media and were shaken at 250 rpm and 30 °C for two to three days. The seed cultures were then transferred to 45 mL glass tubes

containing 15 mL of fresh media with a starting OD_{600} of 0.2. Maximal MA production was observed at about 96 hours.

1.7 *In vivo* PCA decarboxylase activity

The activity of PCA decarboxylase was assessed at different levels of dissolved oxygen. Three different oxygen scenarios were tested: a) aerobic b) oxygen-limited, and c) anaerobic. The aerobic culture was carried out in a 250 mL baffled flask with 25 mL of media with shaking at 250 rpm and 30 °C. The oxygen-limited and anaerobic cultures were carried out in 100 mL serum bottles containing 60 mL media with shaking at 150 rpm and 30 °C. The oxygen-limited flasks were covered with aluminum foil, whereas the anaerobic cultures were cap-sealed. A plasmid containing only the *aroY* cassette was assembled in pRS414 plasmid and transformed into InvSc1, yielding strain InvSc1 pRS414 *aroY* (Table S1) for this test.

The seed culture was grown for two days and transferred to the corresponding flask with an initial OD_{600} of 0.2. After 24 hours of growth, the cultures were spiked with 1 mM PCA. After 18 hours, samples were taken to measure the conversion of PCA to catechol. The values of catechol were normalized by OD_{600} values.

1.8 Scale-up fermentation

An Applikon Biotechnology mini-fermenter system (Netherlands) equipped with a 250 mL vessel was implemented for scale-up fermentation to optimize MA production with strain InvSc1 MA4. 4 mL of initial culture was used as a seed to inoculate the fermenter at a starting OD_{600} of 0.2 (working volume was 200 mL). Temperature was maintained at 30 °C, the agitation was set to 500 rpm, and the percentage of dissolved oxygen was controlled by pumping air. All the parameters were manipulated with a built-in process control software *my*-control. Control of pH was not required for these experiments. The BioXpert Lite software was used for online monitor and data acquisition. All cultures were carried out for 5 days and samples were collected every 24 hours.

1.9 Metabolite detection

An ACQUITY Ultra performance Liquid Chromatography from Waters (Millford, MA) equipped with a BEH-C18 column (Waters) and a PDA detector was used for detection of MA

and the pathway intermediates from the fermentation samples. Samples were prepared by centrifugation of 1 mL of fermentation broth at 5,000 rpm for 5 minutes. The supernatant was diluted 10 times in nanopure water and filtered with a 2 μm syringe filter. The mobile phase consisted of 0.2% formic acid in nanopurewater (Solution A) and 0.2% formic acid in acetonitrile (Solution B). The method was as follows: 0.6 ml min^{-1} of 3% Solution A and 97% Solution B for 1.5 minutes, followed by ramping A to 100% (0% B) in 1 minute. From 3 to 3.1 minutes, Solution A was lowered to 3% (97% B) and maintained until minute 5. The column was maintained at 50 °C and the sample reservoir at 4 °C.

Standard solutions for protocatechuic acid (MP Biomedicals, Santa Ana, CA), catechol (Acros Organics, New Jersey, US) and MA (Sigma, St. Louis, MO) were prepared for quantification. Retention times of PCA, catechol, and MA were 0.7 min, 1.1 min, and 1.5 min, respectively. PCA and MA were detected at 259 nm; catechol was detected at 275 nm.

2. Electrocatalytic hydrogenation

The electrochemical studies were conducted in a three-electrode electrochemical cell using a BioLogic VSP-300 potentiostat. The Ag/AgCl in NaCl reference electrode and platinum counter electrode were purchased from BioLogic Science Instruments. The working electrode was purchased from Rotometals (Lead rod, 99.9%). Electrocatalytic hydrogenation experiments were performed in 11 mL of reacting medium with a stir bar at 700 rpm. During the chronoamperometry experiments, 0.5 mL samples of the reaction medium were taken at 5 min, 15 min, 30 min, and 60 min for analysis.

Samples were subsequently analyzed either by ultra-performance liquid chromatography (UPLC) or ^{1}H NMR. For NMR analysis, the samples were dried at room temperature, reconstituted in deuterium oxide, and analyzed with a Bruker 600 MHz NMR spectrometer (AVIII600). UPLC analysis was performed with a Waters H-Class Acquity chromatograph equipped with a HSS C18 Column (1.8 μm, 2.1 x 100 mm) and photo-diode array detector. Samples were prepared by filtration with a 2 μm syringe filter. The mobile phase consisted of a 100% methanol solution (Solution A) and 1% acetic acid (Solution B) in nanopurewater. The method was as follows: 0.35 ml min^{-1} of 4% Solution A and 96% of Solution B for 4.5 min followed by ramping A to 50% (50% B) and maintained until min 6. The composition of the mobile phase was reverted to 4% Solution A and 96% Solution B and maintained for 8 additional min. The column was maintained at 45 °C and the sample reservoir at 15 °C. ACS grade *cis,cis*-

MA was used to synthesize *cis,trans*-MA by heating in water at 75 °C for 25 min. *trans*-HDA (Sigma, St Louis, MO) and *cis,trans*-MA were used for UPLC calibration and as references. Retention times of *cis, trans-MA* and *trans*-HDA are 6.4 min and 4.0 min and were analyzed at 295 nm and 231 nm respectively. Conversions and selectivities, were calculated with the following equations:

$$MA\,Conversion\,(\%) = \left(1 - \frac{[MA]_t}{[MA]_0}\right) * 100$$

$$HDA\ Selectivity\ (\%) = \frac{[HDA]_t}{[MA]_0 - [MA]_t} * 100$$

Voltage and pH studies were performed on MA in K_2SO_4/H_2SO_4 electrolyte solutions in order to keep ionic strength and conductivity constant. A 0.1 M K_2SO_4 with 1.41 mM MA solution was mixed in varying ratios with 0.1 M H_2SO_4 and 1.41 mM MA. The solutions with the specified pH were ECH in the 11 mL small volume cell. In-between experiments, the electrodes were rinsed with DI water and the lead electrode was polished with a kimwipe.

ECH of the fermentation medium was performed as follows. Directly after the fermentation, 11 mL of broth was put in a small volume cell. At the start of the ECH, the surface of a lead electrode was polished with a kimwipe and used as the electrocatalyst. In-between the successive batch reactions, the lead electrode was gently dipped in deionized water, dried, and put in another 11 mL solution of the fermentation medium. In addition, the counter and reference electrodes were washed with deionized water in-between each run. To achieve a 94% yield of 3-hexenedioic acid (HDA) the pH of the fermentation broth was decreased to 2.0 by dropwise adding 0.5 M H_2SO_4. Additionally, the concentration of MA was increased to 2.4 mM.

3 Separations

Recovery of HDA was accomplished by concentrating ~2 L of cell-free fermentation broth containing the highest titer of HDA under basic conditions, followed by activated carbon filtration, and crystallization at reduced pH and temperature. A yield of 67% and a high purity of 98% were obtained (Fig. S7).

Specifically, after removing cells from 2 L fermentation broth, the pH of the cell-free broth was brought from 3 to 8.5 with 10 M NaOH to increase the solubility of HDA. The basic solution was run through a 0.2-µm filter to remove any solid impurities remained in the broth. Following filtration, the broth was concentrated in a vacuum evaporation set up, from ~2 L to 80 mL and re-filtered through a 0.2-µm filter, separating the impurities that precipitated during concentration. The concentrate was then dripped through a 15-mm deep Norit CN1 activated carbon bed (preconditioned with 10 mM NaOH), adsorbing soluble impurities including colorants and odor-causing compounds. The subsequent filtrate was acidified to pH 1.5 using 18.4 M sulfuric acid and crystalized at 4 °C overnight. Crystals of HDA were recovered using vacuum filtration with a Whatman 50 filter, washed with 4 °C 10 mM sulfuric acid, and placed in a desiccator to dryness.

4 Polymer synthesis and characterization

4.1 Polycondensation

The polycondensation reaction between *trans*-HDA and hexamethylenediamine (HMDA) was adapted from the synthesis of nylon 6,6. Specifically, t*rans*-HDA (TCI America) was dissolved in methanol and mixed with a 1:1 mol ratio of HMDA dissolved in methanol. The resulting solution was heated in a round bottom flask at 60 °C. The liquid was decanted from the precipitated salt. The precipitated salt was subsequently washed with methanol, decanted, and left to dry in a fume hood. The solid was then mixed at a 0.86 mass ratio with deionized water. The resulting solution was put in an aluminum weigh pan and heated at 7.5 °C min^{-1} to 250 °C in a tube furnace under flowing ultra-high purity nitrogen. The sample dwelled at the temperature for 30 min before cooling. It was not uncommon during the synthesis of UPA 6,6 to produce a slightly yellow colored polymer. The same synthesis procedure was applied to adipic acid and the HDA purified from the fermentation broth to form nylon 6,6 and UPA 6,6.

4.2 Size Exclusion Chromatography (SEC)

Samples were analyzed by Polyanalytik (London, Canada). Analysis was performed in 0.05 M potassium trifluoroacetate salt in hexafluoro-isopropanol (HFIP). Samples were left to dissolve for 24 h at room temperature under gentle shaking and subsequently injected into a Viscotek TDA302 and GPCmax (ViscoGEl (Inert Mixed-Bed High Molecular Weight GPC Column &

Inert Mixed-Bed Low Molecular Weight GPC Column)) with triple detection analysis. Triple detection analysis consisted of a refractive index, right angle and low angle light scattering, and a four-capillary differential viscometer in series (Table S5, Fig. S8). The absolute molecular weight of nylon 6,6 and UPA 6,6 was calculated using a dn/dc value of 0.235 mL g^{-1}.

4.3 Thermal Gravimetric Analysis (TGA)

TGA analysis of all samples was performed with a Perkin Elmer STA 6000 series thermal gravimetric analyzer (Fig. S9). A small amount of each samples (<20 mg) was placed in a Al_2O_3 crucible and heated from 50 to 850 °C at 10 °C min^{-1} in a 20 ml min^{-1} synthetic air flow.

4.4 Differential Scanning Calorimetry (DSC)

DSC experiments were conducted on a TA-Instruments Q2000 Differential Scanning Calorimeter equipped with a refrigerated cooling system. Three consecutive heating and cooling runs were carried out for each sample (-20 °C to 275 °C) using standard aluminum pans.

4.5 Rheology

A TA Instruments ARES-G2 strain controlled rheometer with a convection oven was used to test the diblocks rheology under nitrogen gas flow to prevent polymer degradation. Samples were tested in a parallel plate geometry using a temperature ramp test at heating rate of 10 °C and a strain of 2%. Melt rheology of UPA 6,6 shows a material with a storage modulus (G') of 18.9 MPa, a loss modulus (G'') of 6.24 MPa at 55 °C and a cross-over modulus at 60 °C (Fig. S11).

4.6 X-ray powder diffraction (XRD)

A SCINTAG XDS2000 powder diffractometer equipped with a Cu source (λ = 1.54 Å) and a Kevex Peltier cooled silicon detector was used to test the nylon 6,6 and the UPA 6,6. A continuous scan mode with a speed of 2.0 deg min^{-1} and a scan range of θ = 5–95 degrees was used for the tests; the scattering wavevector amplitude q and scattering angle θ are related by $q = 4\pi/\lambda \sin\theta$. All samples were finely ground in a ceramic mortar before transfer to a clean blank glass sample holder. Tests were done at room temperature. The XRD pattern of UPA 6,6 showed

a primary diffraction peak with q* at 4.7 $Å^{-1}$ and no higher order peaks (Fig. S12). Nylon 6,6 showed the primary peak at a q* of 4.38 $Å^{-1}$ and a secondary peak at 3.7 $Å^{-1}$.

Table S1. Strains constructed in this study

Strain	Genotype	Plasmid	Parent strain
InvSc1	*MATa his3D1 leu2 trp1-289 ura3-52* *MA*T *his3D1 leu2 trp1-289 ura3-52*	None	None
InvSc1 Δ*pdc1*	*MATa his3D1 leu2 trp1-289 ura3-52* *MA*T *his3D1 leu2 trp1-289 ura3-52* Δ*pdc1*	None	InvSc1
InvSc1 *aro1::aroY*	*MATa his3D1 leu2 trp1-289 ura3-52* *MA*T *his3D1 leu2 trp1-289 ura3-52* *aro1::aroY*	None	InvSc1
InvSc1 pRS414 *aroY*	*MATa his3D1 leu2 trp1-289 ura3-52* *MA*T *his3D1 leu2 trp1-289 ura3-52*	pRS414 *aroY*	InvSc1
InvSc1 MA1	*MATa his3D1 leu2 trp1-289 ura3-52* *MA*T *his3D1 leu2 trp1-289 ura3-52*	pRS425 Sc MA pRS413 $aro4_{K229L}$-*tkl1*	InvSc1
InvSc1 MA2	*MATa his3D1 leu2 trp1-289 ura3-52* *MA*T *his3D1 leu2 trp1-289 ura3-52*	pRS425 Sc MA pRS413 $aro4_{K229L}$-*tkl1* pRS426 WT *aro1*	InvSc1 MA1
InvSc1 MA3	*MATa his3D1 leu2 trp1-289 ura3-52* *MA*T *his3D1 leu2 trp1-289 ura3-52*	pRS425 Sc MA pRS413 $aro4_{K229L}$-*tkl1* pRS426 $aro1_{K1370A}$	InvSc1 MA1
InvSc1 MA4	*MATa his3D1 leu2 trp1-289 ura3-52* *MA*T *his3D1 leu2 trp1-289 ura3-52*	pRS425 Sc MA pRS413 $aro4_{K229L}$-*tkl1* pRS426 $aro1_{D1409A}$	InvSc1 MA1
InvSc1 MA5	*MATa his3D1 leu2 trp1-289 ura3-52* *MA*T *his3D1 leu2 trp1-289 ura3-52*	pRS425 Sc MA pRS413 $aro4_{K229L}$-*tkl1* pRS426 *hdqs-hdqd*	InvSc1 MA1
InvSc1 MA6	*MATa his3D1 leu2 trp1-289 ura3-52* *MA*T *his3D1 leu2 trp1-289 ura3-52*	pRS425 Sc MA pRS413 $aro4_{K229L}$-*tkl1* pRS426 $aro1_{K1370A}$-*hdqs-hdqd*	InvSc1 MA1
InvSc1 MA7	*MATa his3D1 leu2 trp1-289 ura3-52* *MA*T *his3D1 leu2 trp1-289 ura3-52*	pRS425 Sc MA pRS413 $aro4_{K229L}$-*tkl1* pRS426 $aro1_{D1409A}$-*hdqs-hdqd*	InvSc1 MA1
InvSc1 MA8	*MATa his3D1 leu2 trp1-289 ura3-52* *MA*T *his3D1 leu2 trp1-289 ura3-52* *aro1::aroY*	pRS425 Sc MA pRS413 $aro4_{K229L}$-*tkl1* pRS426 $aro1_{D1409A}$	InvSc1 *aro1::aroY*
InvSc1 MA9	*MATa his3D1 leu2 trp1-289 ura3-52* *MA*T *his3D1 leu2 trp1-289 ura3-52*	pRS425 Sc MA pRS413 $aro4_{K229L}$-*tkl1* pRS426 $aro1_{D1409A}$-*pc-ppck*	InvSc1 MA1
InvSc1 MA10	*MATa his3D1 leu2 trp1-289 ura3-52* *MA*T *his3D1 leu2 trp1-289 ura3-52* Δ*pdc1*	pRS425 Sc MA pRS413 $aro4_{K229L}$-*tkl1* pRS426 $aro1_{D1409A}$–*pc-ppck*	InvSc1 Δ*pdc1*

Table S2. **Primers used for gene knockout in S. cerevisiae InvSc1**

Fragment	Primer
aro1-Upstream	F: caacatattctcgatgtgct R: taagataattgtatattacg
aro1-Downstream	F: caataatatatctatccttt R: tacctgttcagtcgatacgt
pdc1-Upstream	F: tttcaatcattggagcaatc R: ataattagagattaaatcgc
pdc1-Downstream	F: tttgattgatttgactgtgt R: agtcagaagagcatacataa

Table S3. **Plasmids constructed in this work.** All plasmids derived from helper plasmids containing constitutive promoters. Heterologous genes were codon optimized for expression in *S. cerevisiae*. Endogenous genes were amplified from *S. cerevisiae* YSG50. The bold underlined codes illustrate the mutation sites. Plasmids were assembled using the DNA Assembler technique [4].

Plasmid	Helper Plasmid	Fragment	Primers 5' --> 3'
pRS425 Sc MA (Plasmid containing the heterologous MA pathway)	pRS425	Backbone	Digest with *EcoR*I
	pRS414 PYKp-*XhoI*-ADH2*t*	PYKp	F: taccgggccccccctcgaggtcgacggtatcgataagcttaatgctactattttggagat
		AROZ	F: tttacaagacaccaatcaaaacaaataaaacatcatcacaatgccatctaagttagcaat
			R: tcttataaagtcaatcatttggcaagcttctcagcaaaccttaaagggcagcacttaatg
		ADH2t	R: acgtattctttgaaatggcgagtattgataatgataaactagctactaataggataaatt
	pRS414 GPDp-*XhoI*-PYK1*t*	GPDp	F: aatttgttataaattcctataatttatcctattagtagctagtttatcattatcaatact
		HQD2	F: ttttttagttttaaaacaccagaacttagtttcgacggatatgtcacaagcttttacaga
			R: ttcaaaaaaataatatcttcattcaatcatgattctttttttataacttaatttcggcgt
		PYK1t	R: gtaaaaaaggagtagaaacattttgaagctatggcgcgcccatttatgtacccatgtata
	pRS414 TEF1p-*XhoI*-HXT7*t*	TEF1p	F: aacttggaaggttatacatgggtacataaatgggcgcgccatagcttcaaaatgtttcta
		AROY	F: aaagaaagcatagcaatctaatctaagttttaattacaaaatgactgcaccaattcaaga
			R: aattagagcgtgatcatgaattaataaaagtgttcgcaaattatttggcggaaccttgat
		HXT7t	R: gcggtggcggccgctctagaactagtggatccggcgcgccataactgactcattagacac
pRS413 *aro4*$_{K229L}$-*tkl1* (Plasmid harboring the mutant *aro4* gene to remove tyrosine feedback inhibition. It also contains the *tkl1* gene to increase the flux in the non-oxidative portion of pentose phosphate pathway)	pRS413	Backbone	Digest with *EcoR*I
	pRS414 TPI1p-*XhoI*-TDH1*t*	TPI1p	F: ctcactatagggcgaattgggtaccgggccccccctcgagtatatctaggaacccatcag
		ARO4$_{K229L}$	F: aactacaaaaaacacatacataaactaaaaatgagtgaatctccaatgttcgctgccaac
			Rmut: tgatagcagcaacaccatg**caa**agtaacacccatgaaatg
			Fmut: catttcatgggtgttact**ttg**catggtgttgctgctatca
			R: aataaaaactaaatcattaaagtaacttaaggagttaaatctatttcttgttaacttctc
		TDH2t	R: tgatgtagtcaaccctcttcttgtttaggatcccatatggcgaaaagccaattagtgtg
	pRS414 ADH1p-*XhoI*-ADH1*t*	ADH1p	F: cttagtatcacactaattggcttttcgccatatgggatcctaaaacaagaagagggttga
		TKL1	F: tcaagctataccaagcatacaatcaactatctcatatacaatgactcaattcactgacat
			R: tggagacttgaccaaacctctggcgaagaagtccaaagctttagaaagctttttttcaaag
		ADH1t	R: gtgcagatgttataatatctgtgcgtgcggccgccatatgcatgccggtagaggtgtggt

Table S3. *Continuation*

pRS426 *aro1*	pRS426 GPDp-*XhoI*-PYK1t	ARO1	F: ttttttagttttaaaacaccagaacttagtttcgacggatatggtgcagttagccaaagt
			R: ttcaaaaaaataatatcttcattcaatcatgattctttttctactctttcgtaacggcat
pRS426 *aro1*$_{K1370A}$	pRS426 GPDp-*XhoI*-PYK1t	ARO1$_{K1370A}$	F: ttttttagttttaaaacaccagaacttagtttcgacggatatggtgcagttagccaaagt
			Rmut: actgcattatatctaa**agc**cagaggaattgtgactgcagc
			Fmut: gctgcagtcacaattcctctg**gct**ttagatataatgcagt
			R: ttcaaaaaaataatatcttcattcaatcatgattctttttctactctttcgtaacggcat
pRS426 *aro1*$_{D1409A}$	pRS426 GPDp-*XhoI*-PYK1t	ARO1$_{D1409A}$	F: ttttttagttttaaaacaccagaacttagtttcgacggatatggtgcagttagccaaagt
			Rmut: aggcattacggatacctaacca**agc**ggtattatcaccctt
			Fmut: aagggtgataatacc**gct**tggttaggtatccgtaatgcct
			R: ttcaaaaaaataatatcttcattcaatcatgattctttttctactctttcgtaacggcat
pRS426 *dhqs-dhqd*	pRS414 TEF1p-*XhoI*-HXT7t	TEF1p	F: aagaactaacttggaaggttatacatgggtacataaatgaatagcttcaaaatgtttcta
		DHQD	F: aaagaaagcatagcaatctaatctaagttttaattacaaaatggaaagaatcgttgttac
			R: aattagagcgtgatcatgaattaataaaagtgttcgcaaactcgagttaagcagattggc
		HXT7t	R: attgttttgtactgagattaatctccaaaatagtagcattataactgactcattagacac
	pRS414 PYKp-*XhoI*-ADH2*t*	PYKp	F: ctgtatcccgcttcaaaaagtgtctaatgagtcagttataatgctactattttggagatt
		DHQS	F: tttacaagacaccaatcaaaacaaataaaacatcatcacaatgaagaccgttaccgttaa
			R: tcttataaagtcaatcatttggcaagcttctcagcaaaccttaggcttgatgcaatatgg
		ADH2t	R: taatttatcctattagtagctcctgcagcccgggggatccactagttctagagcggccgc
pRS426 *aro1*$_{K1370A}$-*dhqs-dhqd*	pRS426 *aro1*$_{K1370A}$	GPDp-ARO1$_{K1370A}$-PYK1t	Digest with *BamH*I
	pRS426 *dhqs-dhqd*	TEF1p-DHQS -HXT7t	Digest with *Afl*II
		PYKp-DHQD-ADH2t	
pRS426 *aro1*$_{D1409A}$-*dhqs-dhqd*	pRS426 *aro1*$_{D1409A}$	GPDp-ARO1$_{D1409A}$-PYK1t	Digest with *BamH*I
	pRS426 *dhqs-dhqd*	TEF1p-DHQS-HXT7t	Digest with *Afl*II
		PYKp-DHQD-ADH2t	

Table S3. *Continuation.*

pRS426 *aro1*$_{D1409A}$-*pc*-*ppck* (Plasmid harboring the mutant *aro1* gene, as well as pyruvate carboxylase and phosphoenolpyruvate carboxykinase for pyruvate recycling to PEP)	pRS426 *aro1*$_{D1409A}$	GPDp-ARO1$_{D1409A}$-PYK1t	Digest with *BamH*I
	pRS414 TEF1p-*XhoI*-HXT7t	TEF1p	F: aagaactaacttggaaggttatacatgggtacataaatgaatagcttcaaaatgtttcta
		PC	F: aaagaaagcatagcaatctaatctaagttttaattacaaaatgtcgcaaagaaaattcgc
			R: agcgtgatcatgaattaataaaagtgttcgcaaactcgagtcatgccttagtttcaacag
		HXT7t	R: attgttttgtactgagattaatctccaaaatagtagcattataactgactcattagacac
	pRS414 PYKp-*XhoI*-ADH2*t*	PYKp	F: ctgtatcccgcttcaaaaagtgtctaatgagtcagttataatgctactattttggagatt
		PPCK	F: tttacaagacaccaatcaaaacaaataaaacatcatcacaatgtccccttctaaaatgaa
			R: tcttataaagtcaatcatttggcaagcttctcagcaaaccttactcgaattgaggaccag
		ADH2t	R: gcggccgctctagaactagtggatcccccgggctgcaggagctactaataggataaatta

Table S4. Physiological parameters of the InvSc1 wildtype and knockout strains.

Strain	μ max (h^{-1})	$Y_{x/s}$ (g biomass g^{-1}glucose)
InvSc1 *wt*	0.38 ± 0.017	0.27 ± 0.010
InvSc1 *aro1::aroY*	0.27 ± 0.010	0.12 ± 0.006
InvSc1 Δ*pdc1*	0.39 ± 0.016	0.27 ± 0.010

Table S5. Triple detection SEC results of triplicate injections of UPA 6,6. Average recovery of all injection was 101.05 ± 0.72 %

Sample ID	Injection	V_{peak} (mL)	M_n (Da)	M_w (Da)	M_z (Da)	M_w/M_n (PDI)	[η] (dl/g)	R_h (nm)	M-H α	M-H Log K
	1	14.831	11,516	40,156	237,526	3.487	0.3142	5.124	0.525	-2.823
	2	14.826	10,255	39,336	349,171	3.836	0.3131	5.057	0.519	-2.794
UPA	3	14.819	14,941	41,165	175,890	2.755	0.3097	5.24	0.551	-2.961
6,6	**Average**	**14.825**	**12,237**	**40,219**	**254,196**	**3.359**	**0.3123**	**5.14**	**0.532**	**-2.859**
	σ	0.0049	1,980	748	71,717	0.45	0.0019	0.08	0.014	0.073
	% RSD	0.03%	16.18%	1.86%	28.21%	13.40%	0.61%	1.47%	2.61%	2.55%
	1	14.924	15,958	35,568	95,554	2.229	0.4538	5.831	0.573	-2.884
	2	14.968	19,547	37,217	95,573	1.904	0.4470	5.941	0.579	-3.006
Nylon	3	14.891	17,951	36,057	98,070	2.009	0.4592	5.900	0.580	-2.915
6,6	**Average**	**14.928**	**17,819**	**36,281**	**96,399**	**2.047**	**0.4533**	**5.890**	**0.583**	**-2.935**
	σ	0.0315	1,468	692	1,182	0.135	0.0050	0.05	0.010	0.052
	% RSD	0.21%	8.24%	1.91%	1.23%	6.61%	1.10%	0.77%	1.73%	1.76%

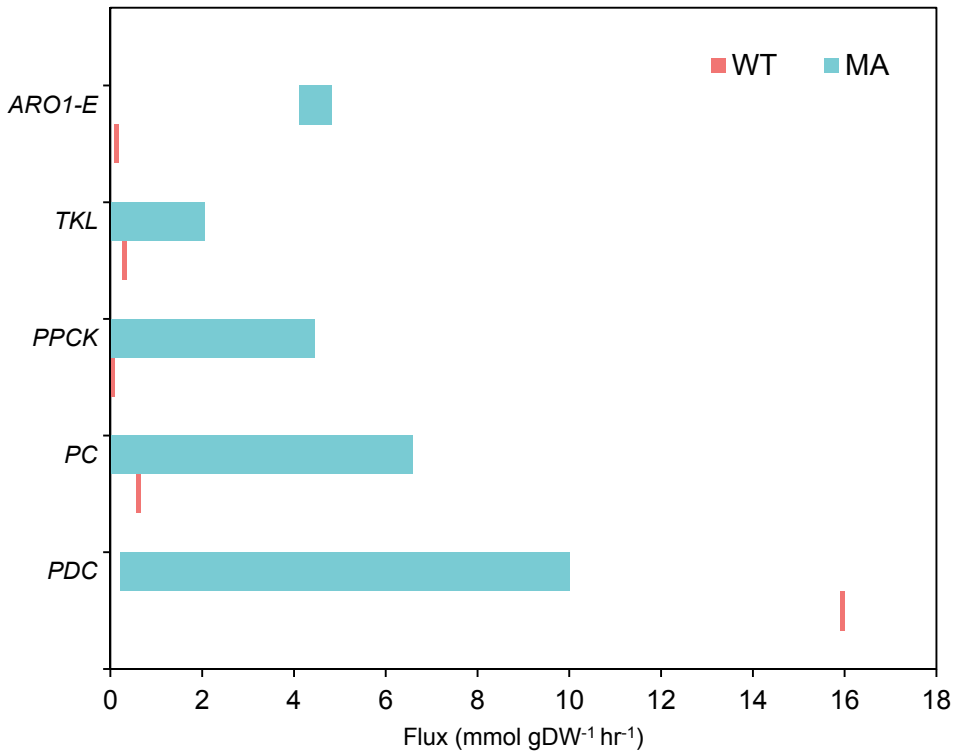

Fig. S1. *In silico* modeling of MA production in *S. cerevisiae*. Flux variability analysis was performed under two different scenarios. WT represents the flux through selected reactions targeting maximal biomass production. Similarly, the MA scenario represents the flux through the selected reactions having maximal MA as target while maintaining 20% of the maximum theoretical biomass. The bars separated from the y-axis indicate that for those reactions, the model predicted a non-zero value to meet the constraints set. Note FBA analysis normally leads to multiple mathematic solutions. For example, the flux of PDC in the WT strain should be maintained around 15.95 mmol gDW^{-1} hr^{-1} to achieve the optimal biomass level, whereas the flux values of PDC in a range of 0.2 to 9.8 mmol gDW^{-1} hr^{-1} could all satisfy the purpose of maximizing MA production. Nevertheless, the majority of the solutions indicate that Aro1E, TKL, PPCK, and PC need to be up-regulated and PDC needs to be down-regulated. The following abbreviations are used: *ARO1E:* subunit of *ARO1* catalyzing 3-dehydroquinate dehydration; *TKL:* transketolase; *PPCK:* phosphoenolpyruvate carboxykinase; *PC:* pyruvate carboxylase; *PDC:* pyruvate decarboxylase.

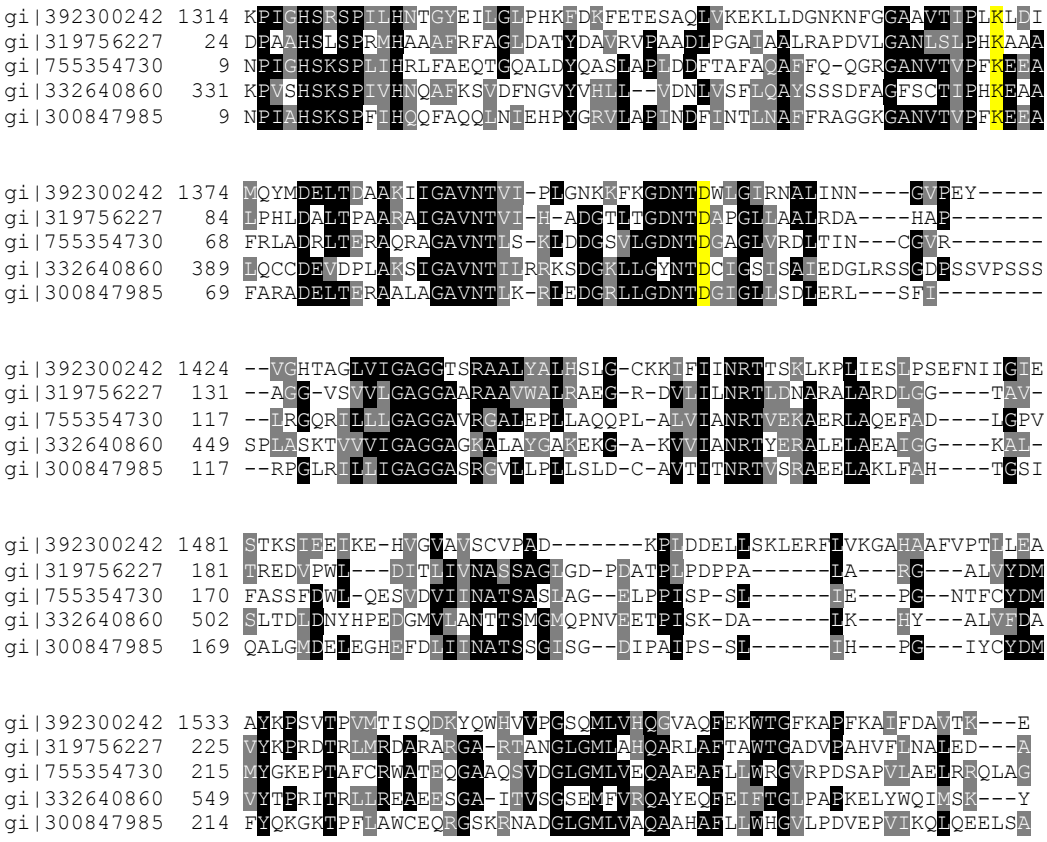

Fig. S2. Sequence alignment of ARO1D with shikimate dehydrogenases from various species. The ARO1 pentafunctional enzyme from *S. cerevisiae* (gi: 392300242) was aligned with sequences from *Deinococcus maricopensis* (gi: 319756227), *Pseudomonas viridiflava* (gi: 755354730), *Arabidopsis thaliana* (gi: 332640860), and *E. coli* (gi: 300847985). The residues K1370 and D1409 in ARO1 (yellow) showed 100% homology among all the species. These amino acids have been previously characterized in species like *E. coli and A. thaliana,* and represent critical residues for efficient catalytic activity. Thus, they were subjected to mutagenesis in our work to stop the conversion of DHS into shikimate.

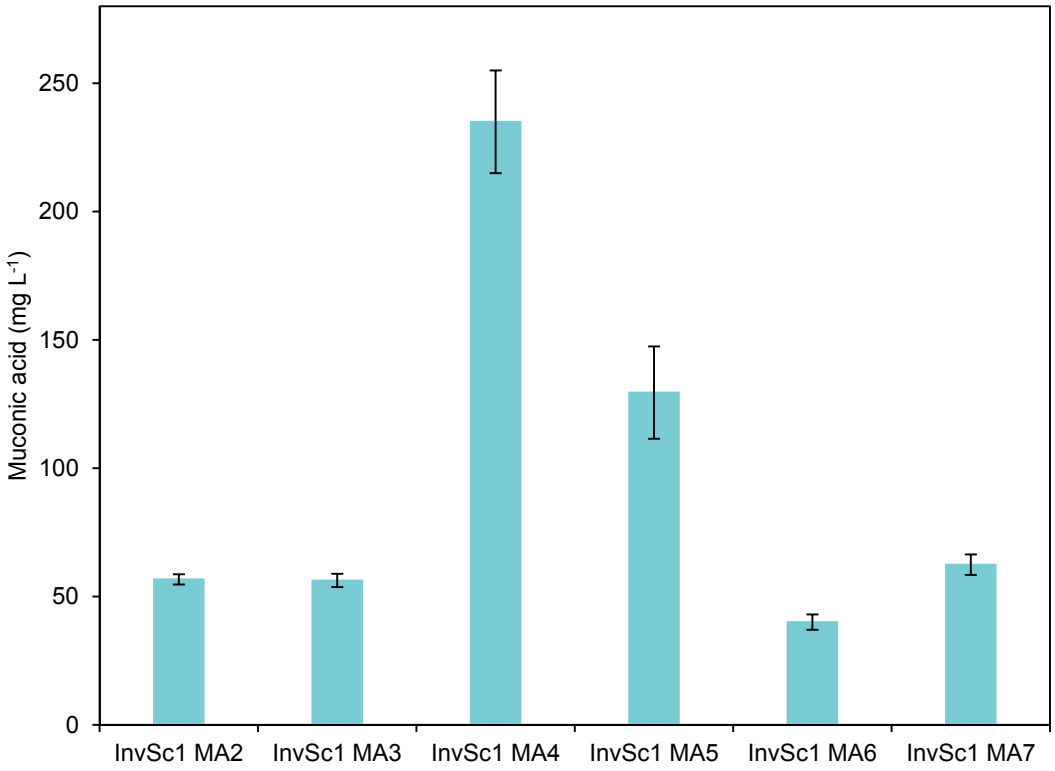

Fig. S3. Characterization of a panel of plasmids carrying *aro1* variants and the *E.coli* genes *dhqd* and *dhqs*. Accumulation of PCA and MA was quantified in strains harboring plasmids with different *aro1* mutants. Strains were grown in 15 mL of SC-LHU supplemented with 4% glucose for 96 hours. Error bars represent the standard deviation of three biological replicates.

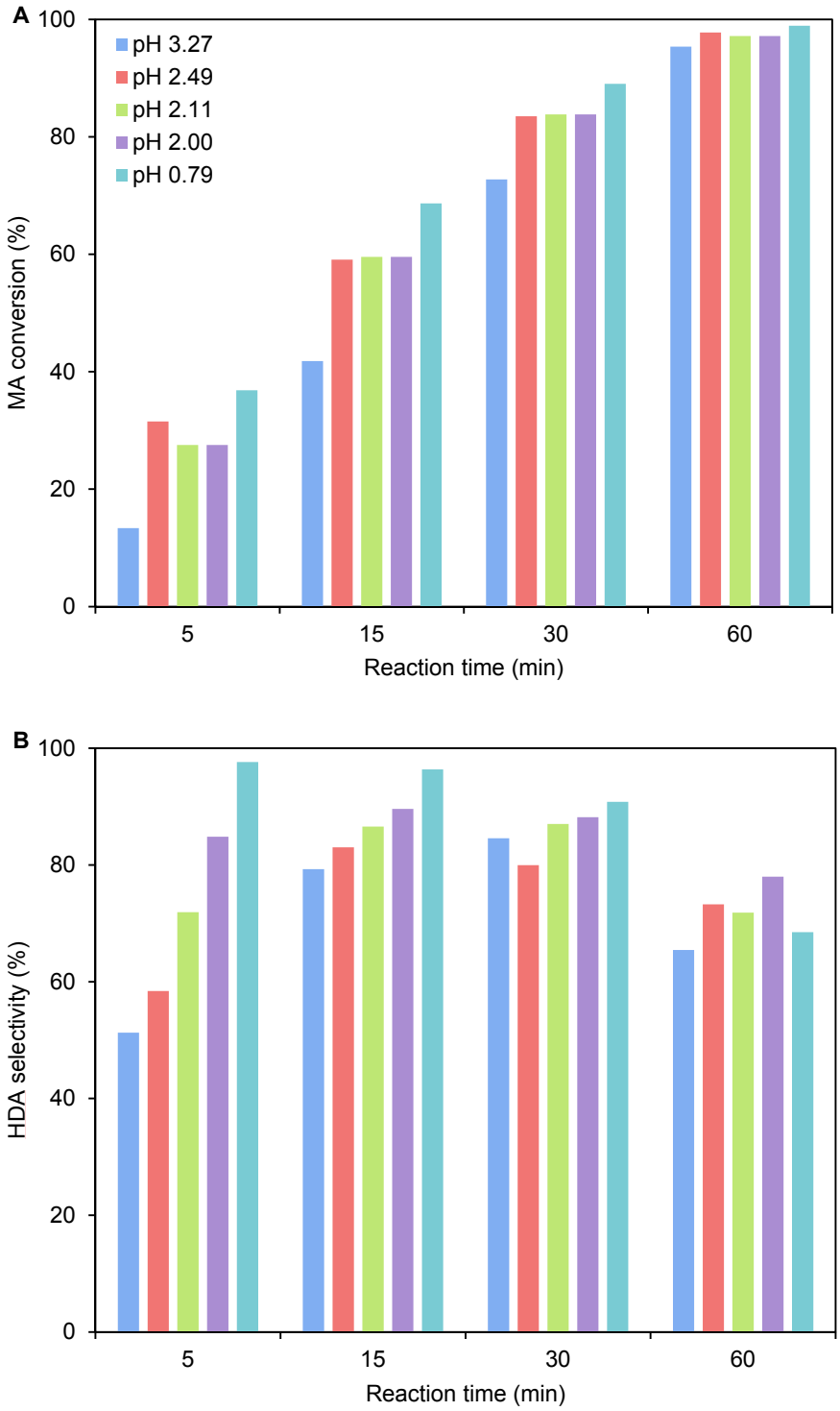

Fig. S4. ECH of model solutions of MA with varying pH. The pH in the solution was changed by adding various ratios of K_2SO_4 and H_2SO_4 to maintain the ionic conductivity. An ECH of the solution was run at -1.5 V for 1 h with the Pb catalyst. (**A**) MA conversion and (**B**) HDA selectivity.

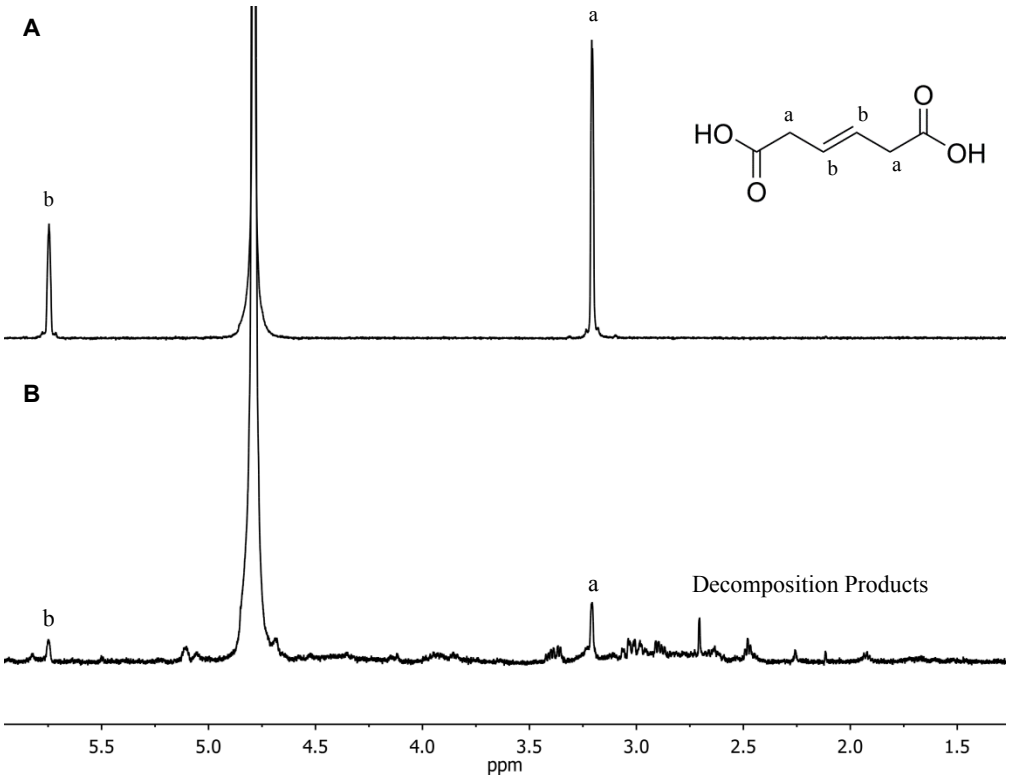

Fig. S5. ^{1}H NMR spectra, 600 MHz, D_2O, of HDA subjected to -1.5 V for 2 h before (**A**) and after (**B**) reaction. Decomposition products are shown to form after the reaction.

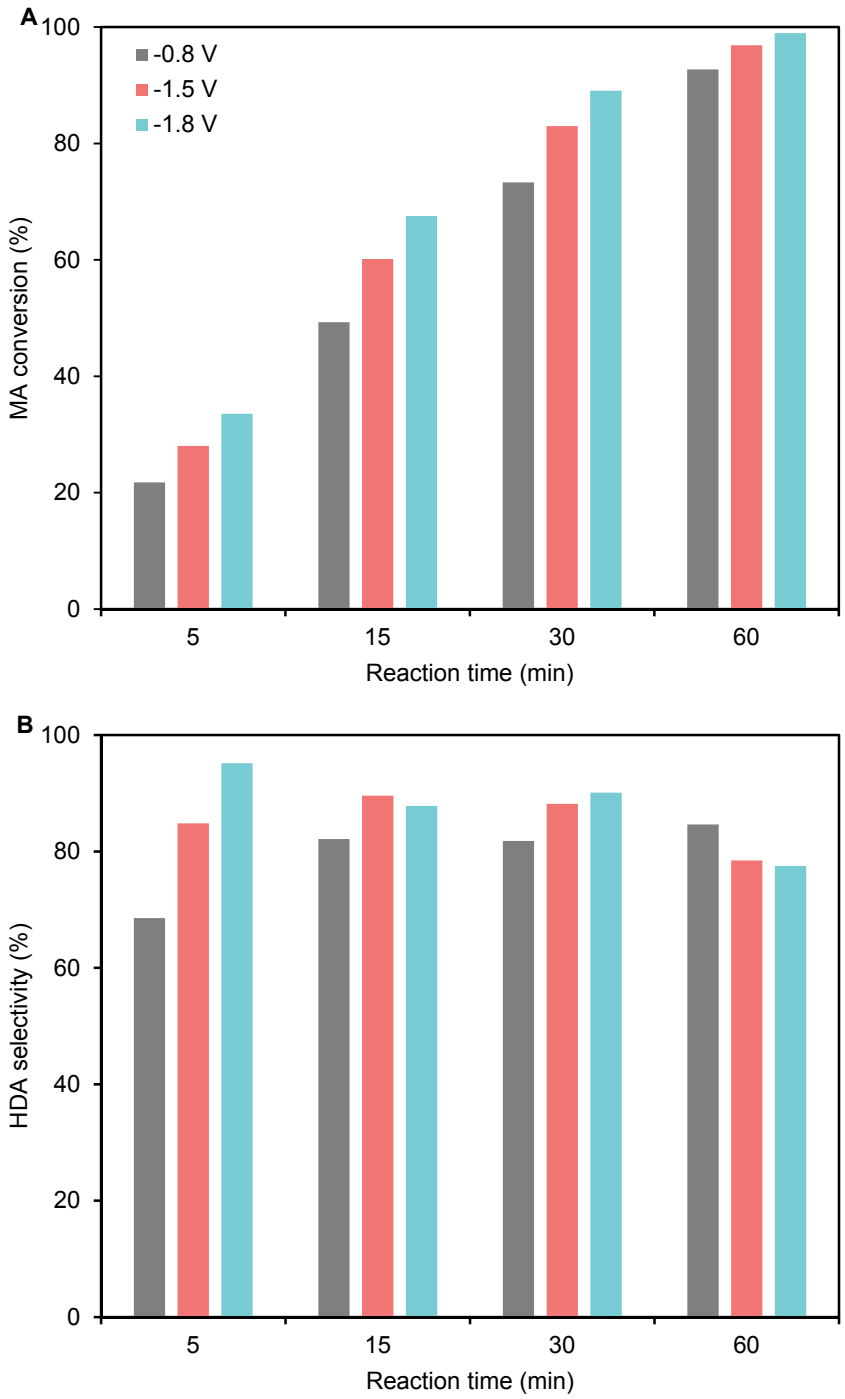

Fig. S6. ECH of model solutions of MA at varying potentials. The pH was fixed at 2.0 by adding 0.5 M H_2SO_4 to a solution of water and MA. An ECH of the solution was run for 1 h with the applied potentials.

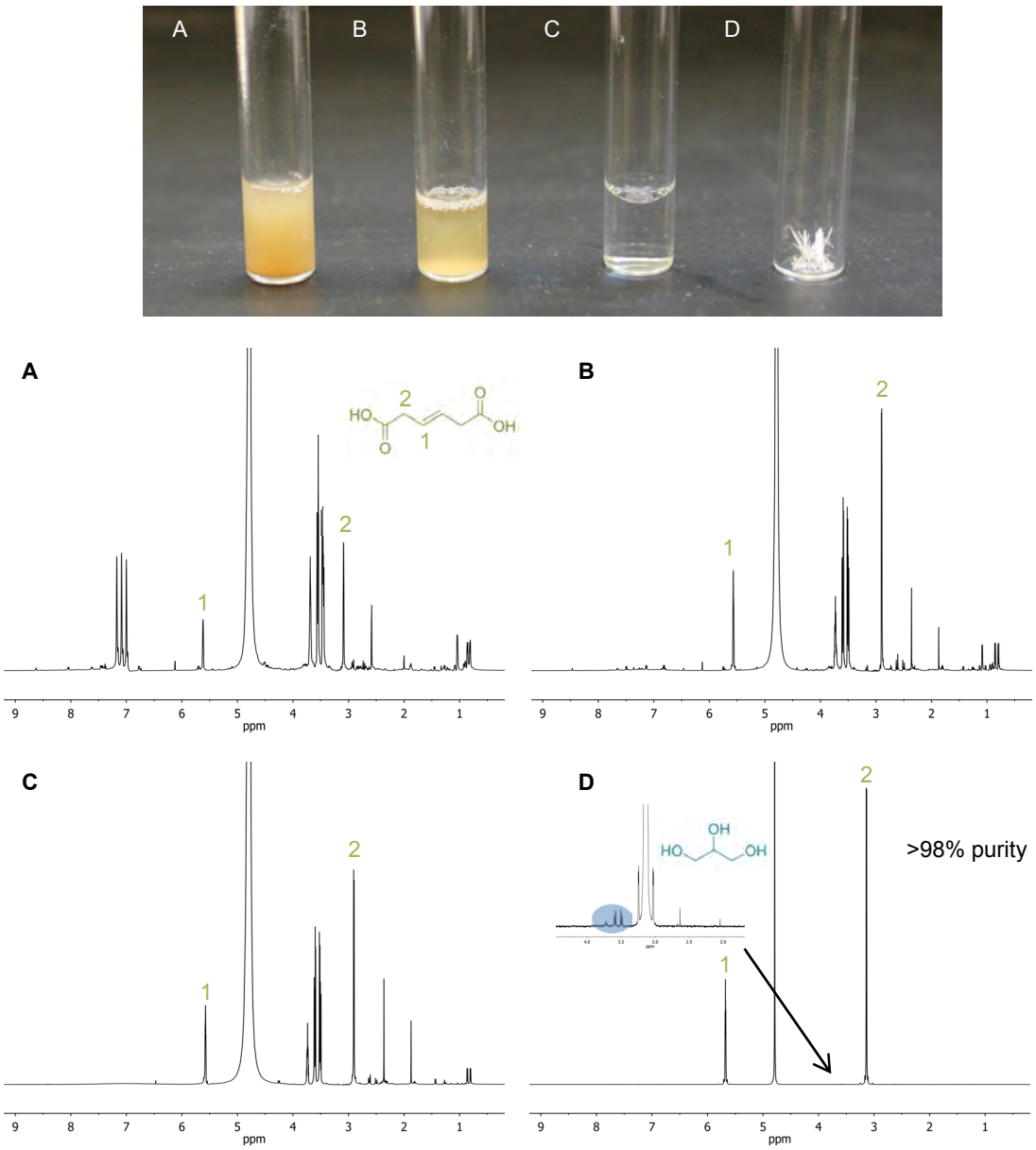

Fig. S7. Photographs and ^{1}H NMR spectra, 600 MHz, D_2O during the separation of HDA following fermentation. The fermentation broth containing HDA was concentrated through distillation at pH 8.5 (A). After concentration, the solid products were removed with a 0.2-µm filter (B) and the following solution was purified with activated carbon (C). Following the purification, HDA was recovered by crystallization at pH 1.5 and 4°C overnight (D). Purity was obtained through liquid chromatography with a photodiode array detector.

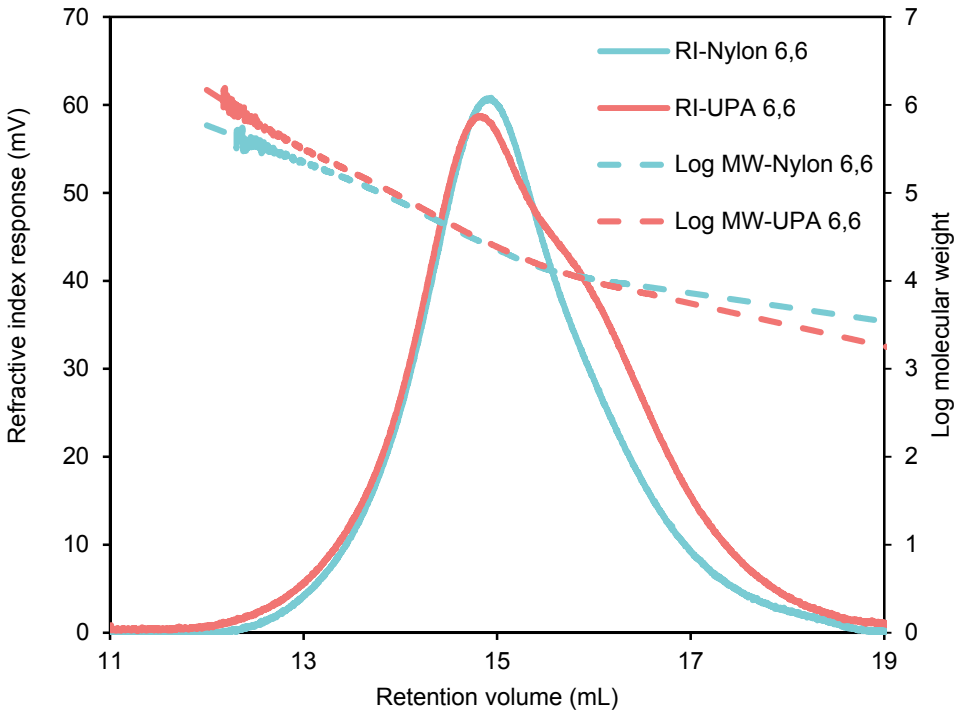

Fig. S8. Overlay from GPC elution traces obtained from RI detector and Log MW (diagonal lines) versus retention volume.

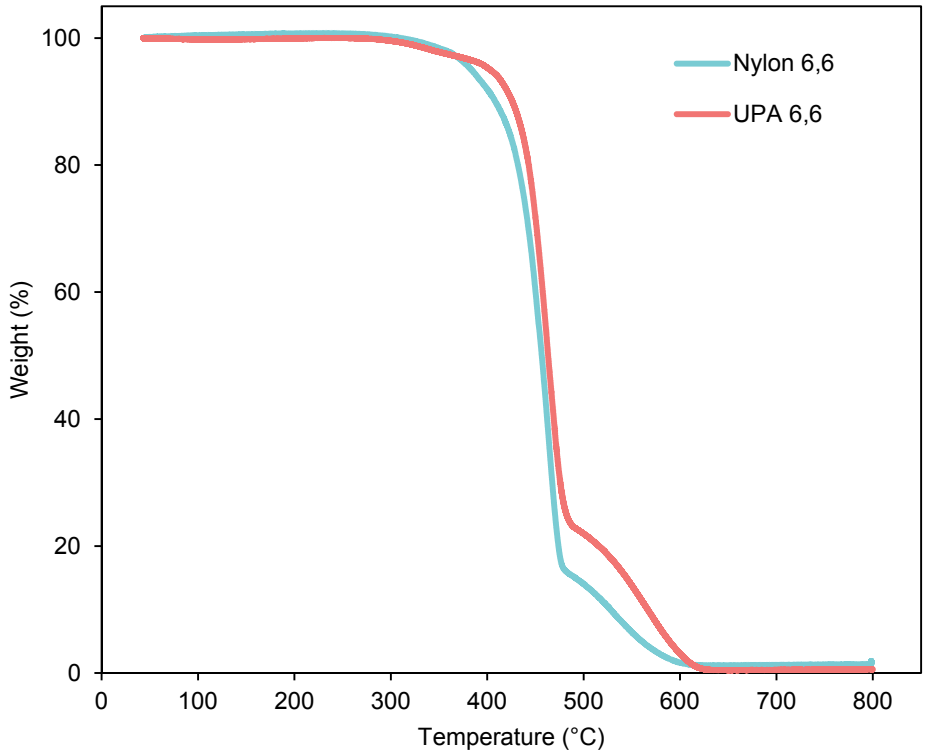

Fig. S9. Thermal gravimetric analysis of nylon 6,6 and UPA 6,6. Nylon 6,6 displays 50% mass loss at 456 °C and UPA 6,6 displays a 50% mass loss at 463 °C.

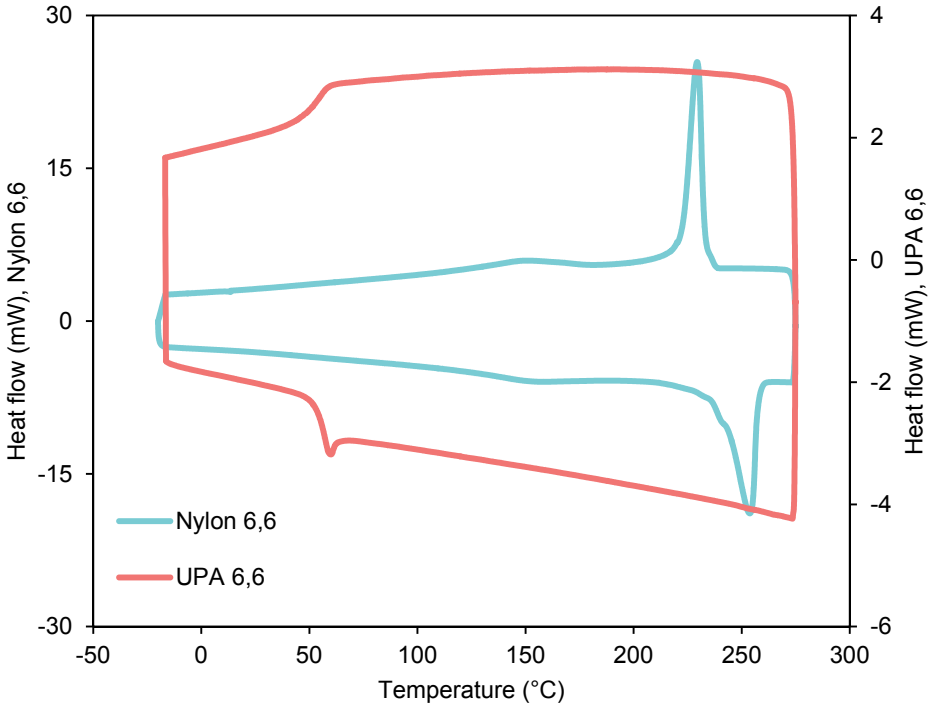

Fig. S10. Differential scanning calorimetry (exothermic up) displayed melting temperature of 255 °C for nylon 6,6 and 60 °C for UPA 6,6.

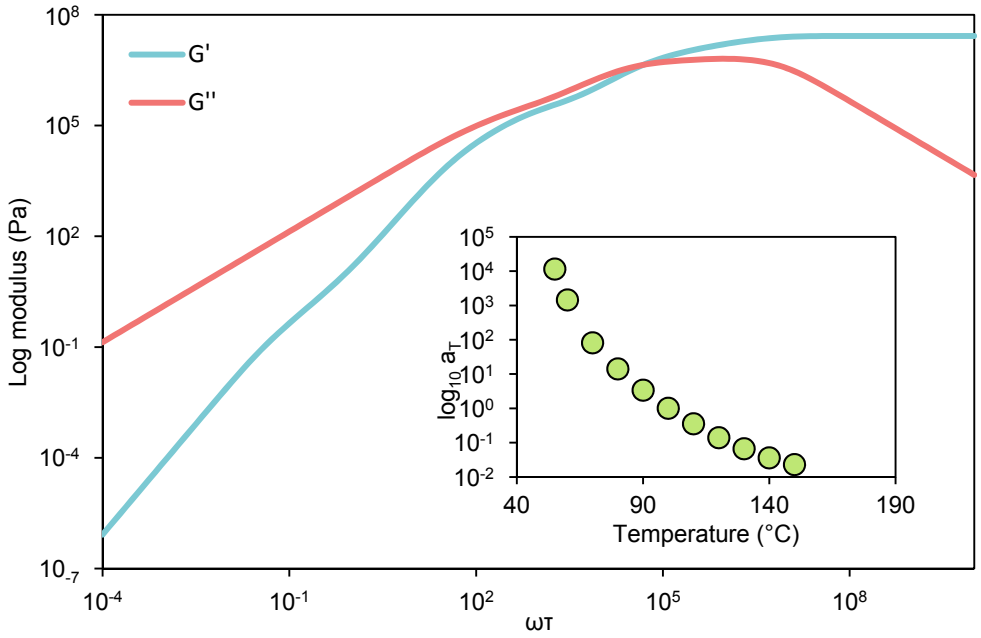

Fig. S11. Master curve of the dynamic shear moduli *G'* and *G''* for UPA 6,6 over the temperature range 50–150 °C (reference temperature is T_{ref} = 100 °C). The material shows classical Rouse-like behavior, common in linear low molecular weight polymer melts. The inset shows the temperature dependence of time-temperature superposition shift factors, which fit to the Williams-Landel-Ferry model with C_1 = 4.9 and C_2 = 100.84 °C.

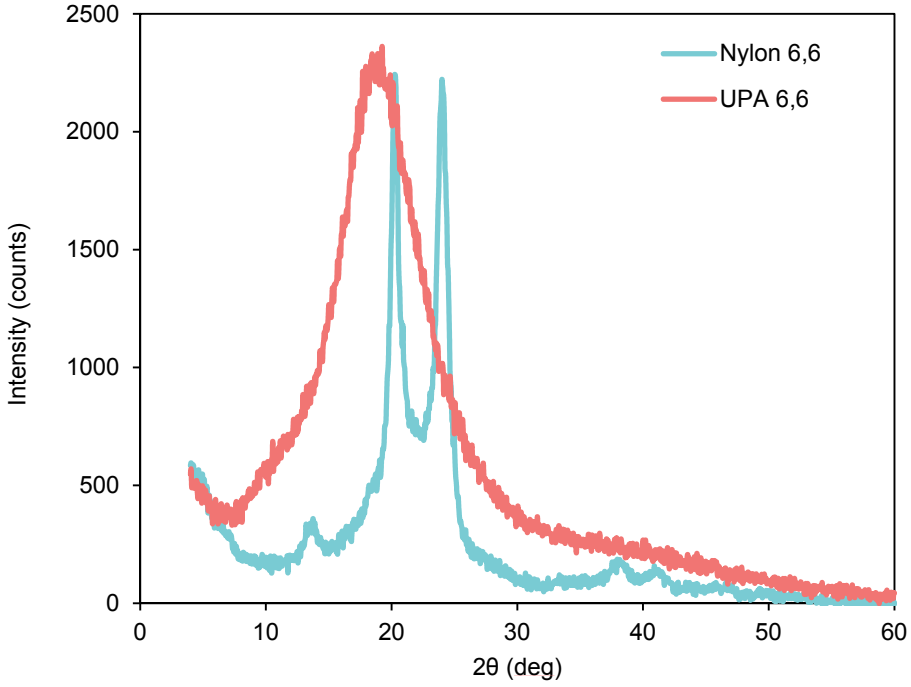

Fig. S12. XRD pattern of UPA 6,6 showing the primary diffraction peak with a q* at 4.7 $Å^{-1}$ and no higher order peaks. Nylon 6,6 shows the primary peak at a q* of 4.38 $Å^{-1}$ and a secondary peak at 3.7 $Å^{-1}$.

References

[1] J. Schellenberger, R. Que, R. M. T. Fleming, I. Thiele, J. D. Orth, A. M. Feist, D. C. Zielinski, A. Bordbar, N. E. Lewis, S. Rahmanian, J. Kang, D. R. Hyduke, B. O. Palsson, *Nat. Protoc.* **2011**, *6*, 1290.

[2] M. L. Mo, B. O. Palsson, M. J. Herrgard, *BMC Syst. Biol.* **2009**, *3*, 37.

[3] K. A. Curran, J. M. Leavitt, A. S. Karim, H. S. Alper, *Metab. Eng.* **2013**, *15*, 55.

[4] Z. Shao, H. Zhao, H. Zhao, *Nucleic Acids Res.* **2009**, *37*, e16.

Biorefinery

International Edition: DOI: 10.1002/anie.201509653
German Edition: DOI: 10.1002/ange.201509653

Combining Metabolic Engineering and Electrocatalysis: Application to the Production of Polyamides from Sugar

Miguel Suastegui[+], John E. Matthiesen[+], Jack M. Carraher, Nacu Hernandez, Natalia Rodriguez Quiroz, Adam Okerlund, Eric W. Cochran, Zengyi Shao, and Jean-Philippe Tessonnier**

Abstract: *Biorefineries aim to convert biomass into a spectrum of products ranging from biofuels to specialty chemicals. To achieve economically sustainable conversion, it is crucial to streamline the catalytic and downstream processing steps. In this work, a route that combines bio- and electrocatalysis to convert glucose into bio-based unsaturated nylon-6,6 is reported. An engineered strain of Saccharomyces cerevisiae was used as the initial biocatalyst for the conversion of glucose into muconic acid, with the highest reported muconic acid titer of 559.5 mg L^{-1} in yeast. Without any separation, muconic acid was further electrocatalytically hydrogenated to 3-hexenedioic acid in 94% yield despite the presence of biogenic impurities. Bio-based unsaturated nylon-6,6 (unsaturated polyamide-6,6) was finally obtained by polymerization of 3-hexenedioic acid with hexamethylenediamine.*

Biomass has emerged as an alternative feedstock to petroleum to render the chemical industry more sustainable and alleviate the concerns associated with fossil resources. The transition from fossil to renewable feedstocks is also expected to revitalize the chemical industry by providing building blocks with new functionalities.[1] Since the U.S. Department of Energy's report on top value-added chemicals from biomass,[2] extensive research has been carried out to establish biological, chemical, or hybrid pathways for converting cellulosic sugars.[3] Over the past few years, it has become evident that building-block diversification requires the combination of biological and chemical transformations,[3b,d,4] that is, biomass is first biologically converted by genetically engineered microbes into platform molecules that are further diversified by chemical catalysis. However, previous attempts to combine chemical and biological processes have led to low conversion rates owing to catalyst deactivation by residual biogenic impurities.[5] The ideal biorefinery pipelines, from biomass to the final products, are currently disrupted by a gap between biological conversion and chemical diversification. We herein report a strategy to bridge this gap with a hybrid fermentation and electrocatalytic process. We illustrate this concept with the conversion of glucose into unsaturated polyamide-6,6 (UPA-6,6). The process entails the fermentation of glucose to muconic acid (MA) followed by electrocatalytic hydrogenation (ECH) to 3-hexenedioic acid (HDA), a monomer that has not been synthesized in high yield through conventional catalytic routes,[6] and subsequent polycondensation with 1,6-hexamethylenediamine (HMDA) to yield the desired UPA-6,6 (Figure 1). The synthesis pipeline developed in this study is based on the utilization of a metabolically engineered yeast and substitution of conventional high-pressure hydrogenation

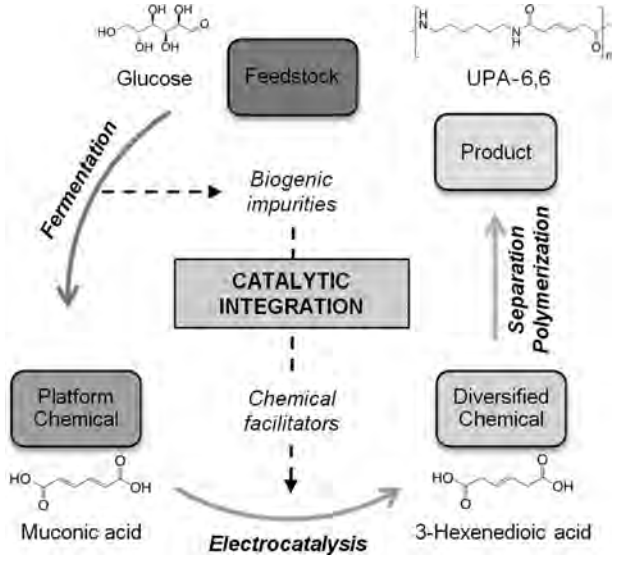

Figure 1. Hybrid conversion of glucose into UPA-6,6. The integration of the catalytic steps was enabled by the compatibility of the process parameters. Replacing conventional high-pressure hydrogenation by direct ECH promoted a seamless flow between the processes, allowing the use of the broth water, salts, and impurities as electrolyte and hydrogen source.

[*] M. Suastegui,[+] J. E. Matthiesen,[+] Dr. J. M. Carraher, Dr. N. Hernandez, Prof. Dr. E. W. Cochran, Prof. Dr. Z. Shao, Prof. Dr. J.-P. Tessonnier
Department of Chemical and Biological Engineering
Iowa State University
Ames, IA 50011 (USA)
E-mail: zyshao@iastate.edu
tesso@iastate.edu

M. Suastegui,[+] J. E. Matthiesen,[+] Dr. J. M. Carraher, N. Rodriguez Quiroz, Dr. A. Okerlund, Prof. Dr. Z. Shao, Prof. Dr. J.-P. Tessonnier
NSF Engineering Research Center for Biorenewable Chemicals (CBiRC)
Ames, IA 50011 (USA)

J. E. Matthiesen,[+] Prof. Dr. J.-P. Tessonnier
US Department of Energy Ames Laboratory
Ames, IA 50011 (USA)

[+] These authors contributed equally to this work.

Supporting information and ORCID(s) from the author(s) for this article are available on the WWW under http://dx.doi.org/10.1002/anie.201509653.

by direct ECH without separation using the broth water, salts, and impurities as electrolyte and hydrogen source. Furthermore, we demonstrate that a biobased polymer can be produced according to this combined bio- and electrocatalytic process.

Muconic acid is the unsaturated synthetic precursor of adipic acid and terephthalic acid, which are the monomers of nylon and polyethylene terephthalate (PET), with a total market value greater than $22 billion.[7] The traditional benzene-based synthetic routes for adipic acid and terephthalic acid are environmentally unfriendly,[8] warranting the need for a sustainable and green production platform. For large-scale fermentation, yeast is the preferred microbial host in industry owing to its unique economic advantages, such as the greater ease in maintaining phage-free culture conditions and the sale of biomass byproducts as animal feeds.[9] Two previous reports showed the heterologous production of MA in *S. cerevisiae* with titers of 1.56 mg L^{-1} [10] and 141 mg L^{-1}.[11] The low production was caused by a combination of low precursor availability, active competing pathway(s), and the presence of rate-limiting enzyme(s). To address these individual issues, we performed flux balance analysis (FBA) to obtain a list of target genes for genetic manipulations (Supporting Information, Figure S1). Figure 2 depicts the metabolic pathway with the key manipulations for enhancing MA production. The details of strain construction in this work are listed in Tables S1–S3.

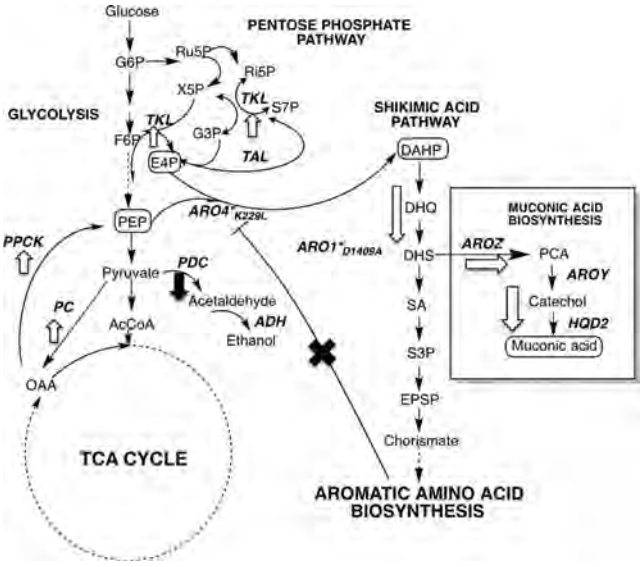

Figure 2. Metabolic engineering rationale for the overproduction of MA in *S. cerevisiae*. Three main strategies were studied: removing the feedback inhibition by aromatic amino acids, increasing the pool of the precursors PEP and E4P, and increasing the pull of carbon into the shikimic acid pathway. Metabolites: G6P: glucose-6-p; F6P: fructose-6-p; Ru5P: ribulose-5-p; Ri5P: ribose-5-p; S7P: sedoheptulose-5-p; X5P: xylulose-5-p; G3P: glyceraldehyde-3-p; AcCoA: acetyl-CoA; PEP: phosphoenolpyruvate; OAA: oxaloacetate; DAHP: 3-deoxy-D-arabinoheptulosonate-7-p; DHQ: 3-dehydroquinate; DHS: 3-dehydroshikimic acid; SA: shikimate; S3P: shikimate-3-p; EPSP: 5-enolpyruvylshikimate-3-p; PCA: protocatechuic acid. White and black arrows represent up- and downregulated reactions, respectively.

The three genes previously characterized in yeast to produce MA from 3-dehydroshikimic acid (DHS), namely *AroZ* from *Podospora anserina*, *AroY* from *Klebsiella pneumoniae*, and *HQD2* from *Candida albicans*,[11] were cloned in a multicopy plasmid. Furthermore, the tyrosine-insensitive DAHP synthase ($ARO4_{K229L}$) was overexpressed to remove feedback inhibition caused by the aromatic amino acids in the growth medium. Following our FBA analysis and previous reports on how to increase the carbon flux into the aromatic amino acid biosynthetic pathway,[11,12] the transketolase gene *(TKL1)* was overexpressed to increase the pool of the precursor erythrose-4-phosphate (E4P). Initial fermentations produced 132 mg L^{-1} MA (strain InvSc1 MA1* in Figure 3a), which is similar to the titer of the previously highest yeast producer MuA12, but the yield was almost doubled.[11] We reasoned that this increase is mostly due to intrinsic differences in the genetic backgrounds of the host strains. Strain dependency in metabolic engineering has also been reported previously.[13] In our case, the strain InvSc1 is a diploid whereas the strain MuA12 derives from the haploid *S. cerevisiae* BY4741.

To further force the carbon flow towards DHS, the flux through the two initial reactions in the aromatic amino acid pathway needs to be increased (Figure 2). As suggested by the FBA (Figure S1), the flux through the DHQ dehydratase had to be increased by a factor of 60 to maximize MA production. In yeast, these two reactions are catalyzed by the pentafunctional ARO1 enzyme,[14] which differs from the stand-alone SA pathway enzymes in bacteria and plants. By sequence alignment of ARO1 with the characterized SA dehydrogenases from various species (Figure S2), it was concluded that the residues K1370 and D1409 could potentially serve as catalytic residues. A panel of plasmids was created to enhance the flux towards DHS and avoid conversion into SA (Figure S3). Overexpression of the mutant $ARO1_{D1409A}$ increased the production of MA to 235 mg L^{-1} (strain InvSc1 MA4), confirming that the residue D1409 is essential for the catalytic activity of the SA dehydrogenase subunit of ARO1. To ensure that no carbon was being diverted to SA, we deleted both copies of *aro1* (InvSc1 MA8 in Figure 3a), but the MA production unexpectedly decreased to 25 mg L^{-1}, and the strain fitness was also affected (Table S4) even when aromatic amino acids were supplemented.

To increase the availability of phosphoenolpyruvate (PEP), we overexpressed *PC* (pyruvate carboxylase) and *PPCK* (phosphoenolpyruvate carboxykinase) in strain InvSc1 MA4, as well as in the strain InvSc1Δ*pdc1* (resulting in the strains InvSc1 MA9 and InvSc1 MA10, respectively). However, the MA titers decreased by around 60% and 74%, respectively (Figure 3a). Recirculation of pyruvate to PEP has been successfully applied in *Escherichia coli* to increase the yield of aromatic compounds.[15] In *S. cerevisiae*, the failure of this strategy might be attributed to the inaccuracy of FBA modeling to predict the compartmentalization fluxes, enzyme kinetics, and the metabolic burden on the cells caused by overexpression of highly regulated genes.

Despite the aforementioned genetic manipulations, the production of MA was still limited by the accumulation of the intermediate protocatechuic acid (PCA). The enzyme PCA

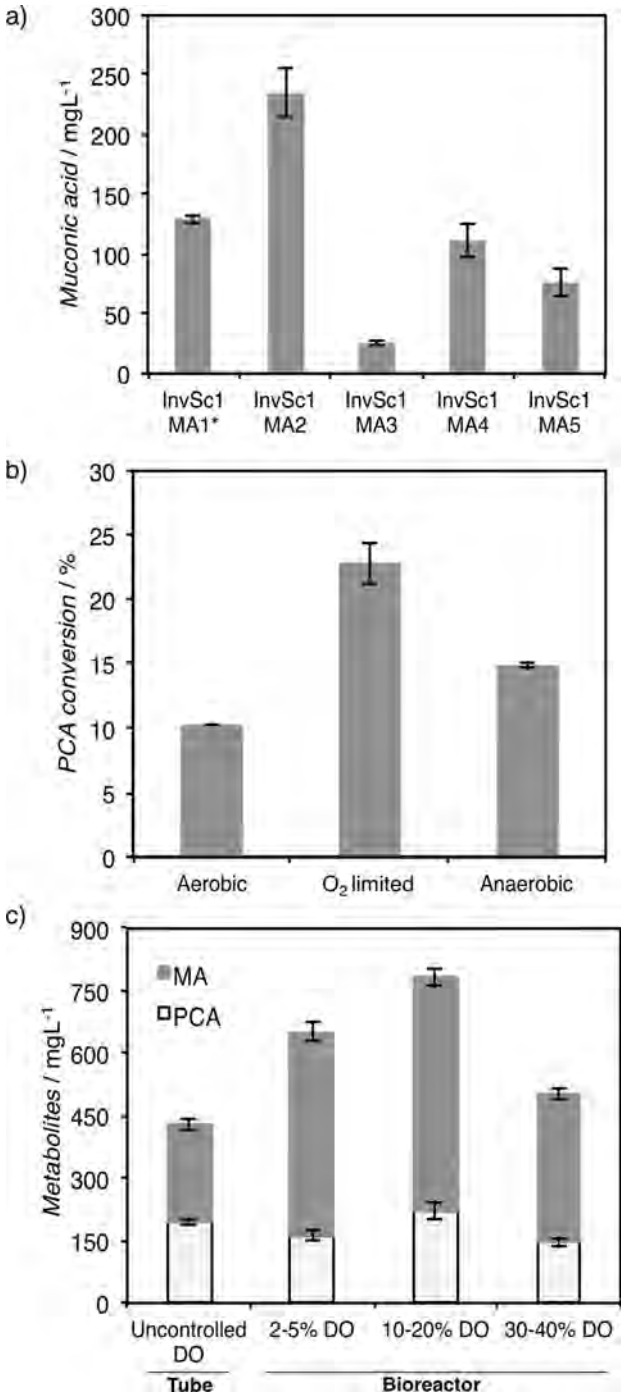

Figure 3. Characterization of MA production in engineered InvSc1 strains. a) MA accumulation in strains grown in glass tubes containing 15 mL of selection media. Maximum MA formation was observed after 96 h of aerobic fermentation. b) PCA decarboxylase activity assay under different oxygen environments. The strain InvSc1 pRS414 aroY was cultured under three different oxygen conditions and spiked with 1 mM PCA after 24 h. The conversions are based on samples collected 18 hours after PCA supplementation. c) Mini-reactor fermentations with the strain InvSc1 MA4 and controlled amounts of dissolved oxygen. The highest MA accumulation was observed when the amount of dissolved oxygen was maintained between 10 to 20% during the first 24 h. After this period, the amount of dissolved oxygen was set to 20% until the end of the fermentation (4 days). *InvSc1 MA1 was grown in 2% glucose, all other strains were grown in 4% glucose.

decarboxylase is known to be oxygen-sensitive;[10,16] we observed that the conversion of PCA into catechol increased by a factor greater than two when the cells were grown in an oxygen-limited culture (Figure 3b). These conditions improved the MA/PCA ratio to 2.5, which is almost five times higher than that of the previously highest MA yeast producer, MuA12.[11] The highest MA titer was 559.5 $mg\,L^{-1}$, representing a fourfold improvement in both titer and yield over strain MuA12 (Figure 3c).

In summary, the MA platform consisted of establishing the heterologous pathway in a diploid yeast strain, overexpressing the novel mutant $ARO1_{D1409A}$, and alleviating the PCA bottleneck with a controlled oxygen environment in the fermentation. The yield of 14 $mg_{MA}\,g_{glucose}^{-1}$ represents the highest value that has been reported for the batch production of aromatic amino acid based metabolites in yeast. Given the strong industrial interest in muconic acid,[17] substantial improvements should be expected in the next several years. Mutagenesis of AroY to remove its oxygen sensitivity[18] and global genetic perturbations[19] coupled with molecular sensor development[20] are potential strategies that will enable yeast to reach the high yields as observed with the *E. coli* platforms.[7b,15b]

The fermentation broth was subsequently hydrogenated in a three-electrode electrochemical cell (Figure 4a). Electrocatalysis was preferred over conventional high-pressure hydrogenation as hydrogen is produced in situ by water splitting, the reaction occurs at ambient temperature and pressure, and the charge on the electrode surface can mitigate poisoning.[21] In this configuration, hydrogen production and MA hydrogenation take place simultaneously at the cathode [Eq. (1) and (2)], enabling a seamless ECH.

$$H^+ + e^- + * \rightarrow H^* \quad (1)$$

$$2\,H^* + C_6H_6O_4 + * \rightarrow C_6H_8O_4 \quad (2)$$

Lead (Pb) was chosen as the catalyst because of its earth abundance, low cost, common use in industrial electrosynthetic applications, metallic state under cathodic potentials, and its stability in the presence of sulfur.[22] The expected resistance to impurities allowed us to significantly simplify the hydrogenation reaction by placing the fermentation broth directly in the electrochemical reactor. The broth contained whole yeast cells, unspent salts, and biogenic impurities arising from cellular metabolism and lysis. The ECH was then allowed to proceed at room temperature and atmospheric pressure for one hour at a potential of −1.5 V vs. Ag/AgCl on a 10 cm^2 lead rod, resulting in 95% MA conversion with 81% selectivity to HDA. To assess the stability of the catalyst in the fermentation medium (in the presence of all potential poisons), five successive one-hour electrocatalytic batch reactions were performed (Figure 4b). Notably, no signs of deactivation were observed, and leaching of the catalyst into the solution was minimal at 6.5 ± 0.4 ppm as determined by elemental analysis.

To further increase the yield of HDA, the effects of pH and applied voltage were investigated independently. A model solution of pure MA dissolved in a potassium sulfate/

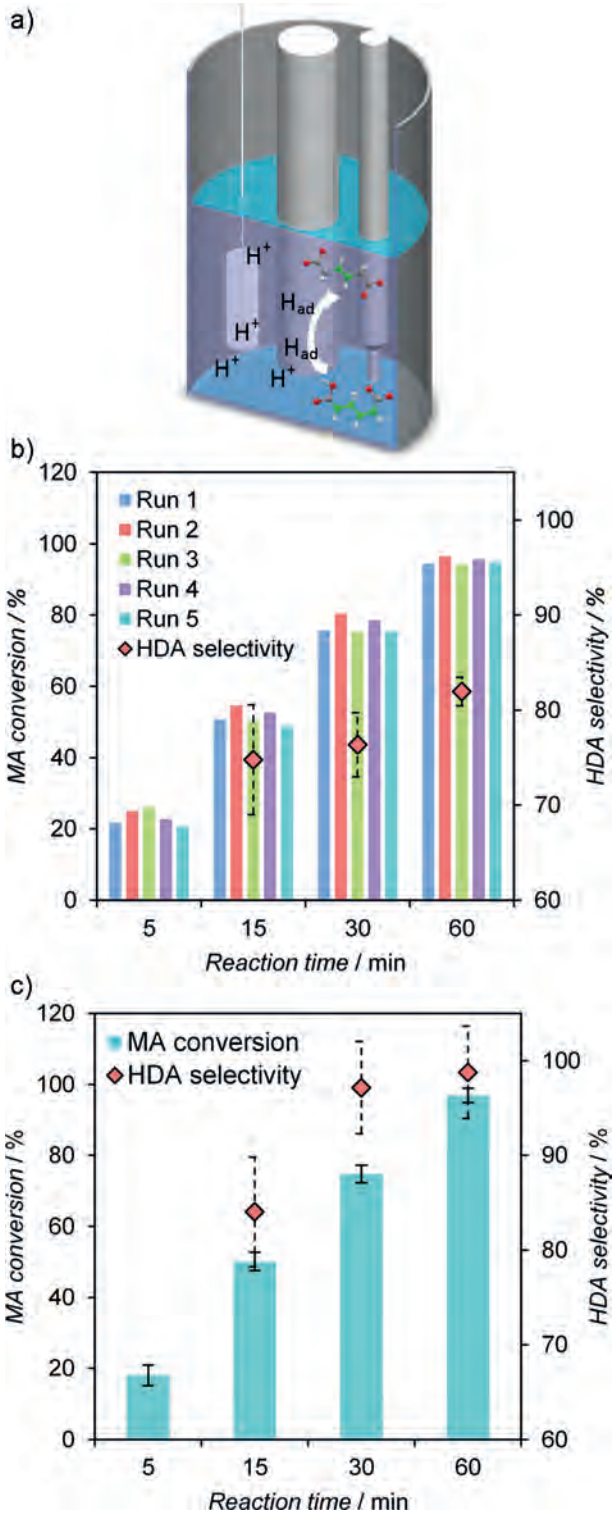

Figure 4. Electrocatalytic hydrogenation of MA to HDA directly in the fermentation broth. The hydrogen necessary for the reaction is generated in situ (H_{ad}) at the surface of the Pb electrode. a) Electrocatalytic single-cell reactor for the conversion of MA into HDA. Carbon gray, hydrogen white, nitrogen blue, oxygen red, C=C bonds green. The reaction was performed at ambient temperature and pressure using a three-electrode electrochemical cell at −1.5 V vs. Ag/AgCl. b) Conversion of MA and average selectivity to the desired product showed no signs of catalyst deactivation when the reaction was repeated five times (runs 1–5). c) MA conversion and HDA selectivity for the ECH (−1.5 V) of the fermentation broth at pH 2.0.

sulfuric acid electrolyte was used to accurately control the ionic strength and to maintain constant ionic conductivity. Acidic conditions favored the selective formation of HDA, especially for reaction times below 30 min (Figure S4). Further ^{1}H NMR analysis of a HDA model solution after ECH revealed that the observed decrease in selectivity as the reaction proceeded was due to the formation of decomposition products through secondary reactions and not due to the formation of additional hydrogenation products, for example, adipic acid (Figure S5). These undesired reactions were enhanced when the pH and/or the applied cathodic voltage were increased (Figure S6). A potential of −1.5 V and a pH of 2.0 offer a compromise between conversion and selectivity.

The conditions optimized with the model solutions were found to also enhance the hydrogenation of the fermentation broth (Figure 4c). Notably, when the pH of the solution was fixed at 2.0, the selectivity towards HDA became 98 ± 4% at 96 ± 2% MA conversion. It is worth noting that the yield achieved for the unpurified broth was actually higher than for the model solution (94% vs. 77%). Whereas catalyst poisoning is a common issue for most of the hydrogenation reactions catalyzed by precious metals,[3d,5,23] it appears that the impurities in the broth were beneficial in our case as they prevented the formation of decomposition products during the ECH.

The reduced decomposition when the fermentation broth is reacted suggests a competitive adsorption process with impurities in solution being sacrificed to minimize potential HDA oxidation. To the best of our knowledge, this is the first time that a biologically produced chemical was hydrogenated in high yield and selectivity directly in the fermentation broth in the presence of diverse impurities.

To demonstrate a full conversion pipeline for the transformation of glucose into a commercially viable product, HDA was separated from the fermentation broth by vacuum evaporation, filtration over activated carbon, and crystallization. High-purity (98%) HDA was obtained in a yield of 67% (Figure S7) and subjected to the final polymerization step. The corresponding saturated nylon-6,6 was synthesized using adipic acid and HMDA in an attempt to compare conventional petrochemical-based nylon-6,6 and bio-based UPA-6,6. The obtained UPA-6,6 consisted of a transparent, partially crystallized material with physical and chemical properties comparable to those of petrochemical nylon (Table 1, Figure 5; see also Table S5, Figure S8–S12). Polymers based on blends of HDA and adipic acid were also synthesized (Figure 5a) to enable different levels of tunability. These HDA-containing nylon materials offer precious grafting sites to tailor the existing nylon grades with desirable properties, for example, crosslinkability, paintability, and flame retardancy.

In conclusion, we have presented a strategy to bridge the gap between biological and chemical catalysis in biorefinery. We have demonstrated its potential by synthesizing a new family of unsaturated polyamides from sugar and anticipate that this strategy will facilitate the incorporation of fermentation and catalytic hydrogenation for a broad range of reactions. Future efforts will be directed towards 1) the scale-up of the hybrid pipeline with a detailed techno-economic

Table 1: The properties of Nylon-6,6 and UPA-6,6.[a]

Property	Nylon-6,6	UPA-6,6
M_n (Da)	17800	12200
PDI	2.0	3.36
T_{melt} [°C]	250	60
Q^* [Å^{-1}]	4.4	4.7
G' [MPa]	–	18.9
G'' [MPa]	–	6.24
G''_c [°C]	–	60

[a] M_n: number average molecular weight; PDI: polydispersity; Q^*: primary diffraction peak; G': storage modulus; G'': loss modulus; G^*_c: crossover modulus.

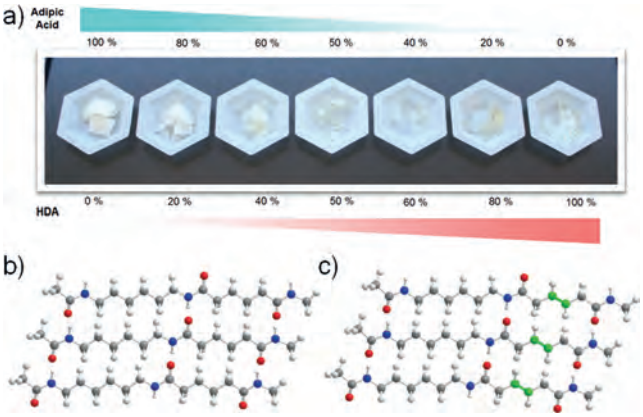

Figure 5. a) Polymer blends of adipic acid and HDA. Percentages are based on the molar ratios of adipic acid and HDA reacted with a 1:1 ratio of HMDA. b, c) Structures of Nylon-6,6 (b) and UPA-6,6 (c), for which petroleum-based adipic acid was substituted with HDA. Carbon gray, hydrogen white, nitrogen blue, oxygen red, C=C bonds green.

analysis to assess the cost efficiency and 2) the integration of the biocatalytic and chemocatalytic reactions into a one-pot process to develop economically and ecologically advantageous synthesis schemes in the context of the water, energy, and food nexus.[4d]

Acknowledgements

We sincerely thank CBiRC for providing the resources that enabled this collaborative work. This material is based upon work supported in part by the National Science Foundation (EEC-0813570 and EPSC-1101284) and the Plant Sciences Institute at Iowa State University. Research at the Ames Laboratory was supported by the U.S. Department of Energy-Laboratory Royalty Revenue (DE-AC02-07CH11358). We thank Dr. Sarah Cady (ISU Chemical Instrumentation Facility) for training and assistance pertaining to the AVIII-600 results included in this publication, Dr. Jieni Lian, Mengguo Yan, Jacob Neff, Jennifer Freeland, Shridharshna Mailachalam, and Andrew Moon for technical assistance, and Taylor Royer for the preparation of Figure 4 A.

Keywords: bio-based polymers · biorefinery · electrocatalysis · metabolic engineering · muconic acid

How to cite: *Angew. Chem. Int. Ed.* **2016**, *55*, 2368–2373
Angew. Chem. **2016**, *128*, 2414–2419

[1] N. Hernández, R. C. Williams, E. W. Cochran, *Org. Biomol. Chem.* **2014**, *12*, 2834.
[2] J. J. Bozell, G. R. Petersen, *Green Chem.* **2010**, *12*, 539.
[3] a) S. Choi, C. W. Song, J. H. Shin, S. Y. Lee, *Metab. Eng.* **2015**, *28*, 223; b) A. Corma, S. Iborra, A. Velty, *Chem. Rev.* **2007**, *107*, 2411; c) J. Becker, C. Wittmann, *Angew. Chem. Int. Ed.* **2015**, *54*, 3328; *Angew. Chem.* **2015**, *127*, 3383; d) T. J. Schwartz, B. J. O'Neill, B. H. Shanks, J. A. Dumesic, *ACS Catal.* **2014**, *4*, 2060.
[4] a) J. G. Linger, D. R. Vardon, M. T. Guarnieri, E. M. Karp, G. B. Hunsinger, M. A. Franden, C. W. Johnson, G. Chupka, T. J. Strathmann, P. T. Pienkos, G. T. Beckham, *Proc. Natl. Acad. Sci. USA* **2014**, *111*, 12013; b) D. R. Vardon, M. A. Franden, C. W. Johnson, E. M. Karp, M. T. Guarnieri, J. G. Linger, M. J. Salm, T. J. Strathmann, G. T. Beckham, *Energy Environ. Sci.* **2015**, *8*, 617; c) B. J. Nikolau, M. A. D. N. Perera, L. Brachova, B. Shanks, *Plant J.* **2008**, *54*, 536; d) H. Gröger, W. Hummel, *Curr. Opin. Chem. Biol.* **2014**, *19*, 171.
[5] a) Z. Zhang, J. E. Jackson, D. J. Miller, *Bioresour. Technol.* **2008**, *99*, 5873; b) T. J. Schwartz, R. L. Johnson, J. Cardenas, A. Okerlund, N. A. Da Silva, K. Schmidt-Rohr, J. A. Dumesic, *Angew. Chem. Int. Ed.* **2014**, *53*, 12718; *Angew. Chem.* **2014**, *126*, 12932.
[6] J. A. Elvidge, R. P. Linstead, J. F. Smith, *J. Chem. Soc.* **1953**, 708.
[7] a) M. J. Burk, R. E. Osterhout, J. Sun, US 20110124911 A1, **2011**; b) W. Niu, K. M. Draths, J. W. Frost, *Biotechnol. Prog.* **2002**, *18*, 201; c) S. Picataggio, T. Beardslee, US8241879 B2, **2012**.
[8] S. Alini, F. Basile, S. Blasioli, C. Rinaldi, A. Vaccari, *Appl. Catal. B* **2007**, *70*, 323.
[9] a) M.-J. In, D. C. Kim, H. J. Chae, *Biotechnol. Bioprocess Eng.* **2005**, *10*, 85; b) T. W. Jeffries, *Curr. Opin. Biotechnol.* **2006**, *17*, 320; c) J. Nielsen, *Science* **2015**, *349*, 1050; d) J. Nielsen, C. Larsson, A. van Maris, J. Pronk, *Curr. Opin. Biotechnol.* **2013**, *24*, 398.
[10] C. Weber, C. Bruckner, S. Weinreb, C. Lehr, C. Essl, E. Boles, *Appl. Environ. Microbiol.* **2012**, *78*, 8421.
[11] K. A. Curran, J. M. Leavitt, A. S. Karim, H. S. Alper, *Metab. Eng.* **2013**, *15*, 55.
[12] a) M. A. H. Luttik, Z. Vuralhan, E. Suir, G. H. Braus, J. T. Pronk, J. M. Daran, *Metab. Eng.* **2008**, *10*, 141; b) K. Li, M. R. Mikola, K. M. Draths, R. M. Worden, J. W. Frost, *Biotechnol. Bioeng.* **1999**, *64*, 61; c) Y.-Y. Cui, C. Ling, Y.-Y. Zhang, J. Huang, J.-Z. Liu, *Microb. Cell Fact.* **2014**, *13*, 21/1.
[13] a) J. Du, Y. Yuan, T. Si, J. Lian, H. Zhao, *Nucleic Acids Res.* **2012**, *40*, e142; b) A. Kümmel, J. C. Ewald, S. M. Fendt, S. J. Jol, P. Picotti, R. Aebersold, U. Sauer, N. Zamboni, M. Heinemann, *FEMS Yeast Res.* **2010**, *10*, 322.
[14] G. H. Braus, *Microbiol. Rev.* **1991**, *55*, 349.
[15] a) R. Patnaik, J. C. Liao, *Appl. Environ. Microbiol.* **1994**, *60*, 3903; b) H. Zhang, B. Pereira, Z. Li, G. Stephanopoulos, *Proc. Natl. Acad. Sci. USA* **2015**, *112*, 8266.
[16] Z. He, J. Wiegel, *J. Bacteriol.* **1996**, *178*, 3539.
[17] a) A. A. Horwitz, J. M. Walter, M. G. Schubert, S. H. Kung, K. Hawkins, D. M. Platt, A. D. Hernday, T. Mahatdejkul-Meadows, W. Szeto, S. S. Chandran, J. D. Newman, *Cell Syst.* **2015**, *1*, 88; b) Y. Rogers, W. Gong, S. Dole, R. Sillers, M. Gandhi, J. Pero, WO2013116244 A1, **2013**.
[18] J. A. Stapleton, J. R. Swartz, *PLoS One* **2010**, *5*, e15275.
[19] a) J. E. DiCarlo, A. J. Conley, M. Penttila, J. Jantti, H. H. Wang, G. M. Church, *ACS Synth. Biol.* **2013**, *2*, 741; b) T. Si, Y. Z. Luo, Z. H. Bao, H. M. Zhao, *ACS Synth. Biol.* **2015**, *4*, 283.

[20] a) S. A. Chugani, M. R. Parsek, A. M. Chakrabarty, *J. Bacteriol.* **1998**, *180*, 2367; b) O. C. Ezezika, L. S. Collier-Hyams, H. A. Dale, A. C. Burk, E. L. Neidle, *Appl. Environ. Microbiol.* **2006**, *72*, 1749.
[21] J. M. Chapuzet, A. Lasia, J. Lessard, *Electrocatalytic Hydrogenation of Organic Compounds*, Wiley, Hoboken, **1998**.
[22] a) R. W. Joyner, K. Kishi, M. W. Roberts, *Proc. R. Soc. London Ser. A* **1978**, *358*, 223; b) D. Pletcher, F. Walsh, *Industrial Electrochemistry*, Springer, Amsterdam, **1993**, p. 481.
[23] J. L. Avalos, G. R. Fink, G. Stephanopoulos, *Nat. Biotechnol.* **2013**, *31*, 335.

Received: October 14, 2015
Published online: January 14, 2016

